Anomalous behavior of water inside the SecY translocon

Sara Capponi[a], Matthias Heyden[b,1], Ana-Nicoleta Bondar[c], Douglas J. Tobias[b], and Stephen H. White[a,2]

[a]Department of Physiology and Biophysics and Center for Biomembrane Systems, University of California, Irvine, CA 92697-4560; [b]Department of Chemistry and Center for Biomembrane Systems, University of California, Irvine, CA 92697-2025; and [c]Theoretical Molecular Biophysics, Department of Physics, Freie Universität Berlin, D-14195 Berlin-Dahlem, Germany

Edited by Michael L. Klein, Temple University, Philadelphia, PA, and approved June 9, 2015 (received for review December 21, 2014)

The heterotrimeric SecY translocon complex is required for the cotranslational assembly of membrane proteins in bacteria and archaea. The insertion of transmembrane (TM) segments during nascent-chain passage through the translocon is generally viewed as a simple partitioning process between the water-filled translocon and membrane lipid bilayer, suggesting that partitioning is driven by the hydrophobic effect. Indeed, the apparent free energy of partitioning of unnatural aliphatic amino acids on TM segments is proportional to accessible surface area, which is a hallmark of the hydrophobic effect [Öjemalm K, et al. (2011) *Proc Natl Acad Sci USA* 108(31):E359–E364]. However, the apparent partitioning solvation parameter is less than one-half the value expected for simple bulk partitioning, suggesting that the water in the translocon departs from bulk behavior. To examine the state of water in a SecY translocon complex embedded in a lipid bilayer, we carried out all-atom molecular-dynamics simulations of the *Pyrococcus furiosus* SecYE, which was determined to be in a "primed" open state [Egea PF, Stroud RM (2010) *Proc Natl Acad Sci USA* 107(40):17182–17187]. Remarkably, SecYE remained in this state throughout our 450-ns simulation. Water molecules within SecY exhibited anomalous diffusion, had highly retarded rotational dynamics, and aligned their dipoles along the SecY transmembrane axis. The translocon is therefore not a simple water-filled pore, which raises the question of how anomalous water behavior affects the mechanism of translocon function and, more generally, the partitioning of hydrophobic molecules. Because large water-filled cavities are found in many membrane proteins, our findings may have broader implications.

membrane protein folding | molecular dynamics | protein-conducting channel | protein hydration | confined water

The heterotrimeric SecY translocon complex (SecYEG in bacteria, SecYEβ in archaea, Sec61αβγ in eukaryotes) is required for the cotranslational assembly of membrane proteins and the secretion of soluble proteins (1–3). The SecY subunit (Fig. 1*A*) has 10 transmembrane helices comprised of two five-helix domains related by pseudo-twofold symmetry around an axis parallel to the membrane (4–8). These helices form an hourglass-shaped water-filled pore that spans the membrane. The so-called hydrophobic pore ring (HR) comprised of six hydrophobic residues forms the narrowest part of the hourglass, located near the bilayer center. Sitting just above the ring on the extracellular side is a small, distorted helix [transmembrane 2a (TM2a)], called the plug domain that is believed to impede the passage of water and solutes across the membrane. Access to the membrane from the water-filled hourglass-shaped interior of SecY is provided by the so-called lateral gate, formed by helices TM2b and TM7 (Fig. 1*A*). SecG is not required for function, but SecE is indispensable. Experimental (9–11) and computational studies (12–15) emphasize the importance of interactions of the gate helices with nascent-chain segments during TM helix insertion.

The general belief is that nascent chains pass through the translocon via the normally closed HR, which must open in response to ribosome docking and nascent-chain elongation. When a TM segment passes through SecY, it is believed that the segment is shunted into the membrane through a simple partitioning process between water-filled SecY and the lipid environment (Fig. 1*B*). Hessa et al. (16, 17) characterized the translocon/membrane insertion energetics and established that the membrane insertion propensity depends on both the hydrophobicity and position of each residue within model TM segments (16, 17). Because the resulting "biological" hydrophobicity scale (16, 17) correlates strongly with physical hydrophobicity scales, translocon/membrane partitioning is believed to be similar to water/membrane partitioning of peptides (18), which is driven by the hydrophobic effect (19).

The hallmark of hydrophobic partitioning is that the favorable partitioning free energy is linearly proportional to the solute nonpolar accessible surface area and is described by the atomic solvation parameter σ (20). For bulk water-to-hydrocarbon partitioning, the solvation parameter typically has a value of about −23 cal·mol^{-1}·Å^{-2} (21). Öjemalm et al. (22) found that the apparent translocon-to-membrane free energy of insertion of nonproteinogenic amino acids at a particular position in the TM segment varied linearly with σ, as expected for hydrophobic-driven partitioning. However, σ was found to be less favorable than that for bulk water/hydrocarbon partitioning and to depend on position within the model TM segment (Fig. 1*B*). Near the ends of the segments, σ ≈ −6 cal·mol^{-1}·Å^{-2}, whereas in the center of the segment σ ≈ −10 cal·mol^{-1}·Å^{-2} (22). These low values of σ caused us to examine the physical behavior of water within the translocon. Specifically, could the water properties within the translocon

Significance

α-Helical membrane proteins are assembled cotranslationally into cell membranes with the aid of the heterotrimeric membrane-embedded translocon complex. The structures of several translocons reveal that the interior has an hourglass shape filled with water. Because nascent peptide chains emerging from the ribosome are thought to pass through the translocon during secretion or membrane insertion, the translocon is often referred to as a protein-conducting channel. We show by all-atom molecular-dynamics simulations that the water molecules within a translocon do not behave as in a bulk phase, which raises fundamental questions not only about the current conceptual model of translocon-assisted insertion of membrane proteins but also about the physical principles of partitioning of solutes between bulk and confined water.

Author contributions: S.C., M.H., A.-N.B., D.J.T., and S.H.W. designed research; S.C. performed research; S.C. and M.H. analyzed data; and S.C., M.H., A.-N.B., D.J.T., and S.H.W. wrote the paper.

The authors declare no conflict of interest.

This article is a PNAS Direct Submission.

[1]Present address: Theoretical Chemistry, Max-Planck-Institut für Kohlenforschung, D-45470 Mülheim an der Ruhr, Germany.

[2]To whom correspondence should be addressed. Email: stephen.white@uci.edu.

This article contains supporting information online at www.pnas.org/lookup/suppl/doi:10.1073/pnas.1424483112/-/DCSupplemental.

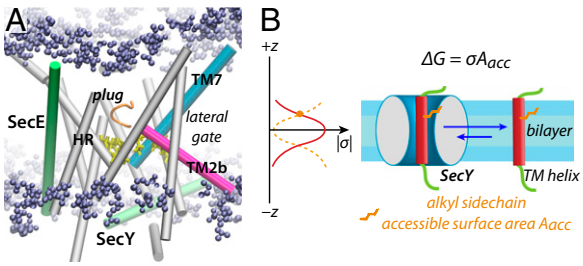

Fig. 1. Structure of *P. furiosus* SecYE and cartoon representation of the translocon-to-lipid bilayer partitioning of a TM helix. (*A*) Structure of SecYE in a lipid bilayer. The lipid headgroups are shown in ice-blue van der Waals representation. The 10 SecY helices are represented in gray cartoon format, except for TM2b (magenta) and TM7 (cyan). The SecE helices are colored green. Hydrophobic ring (HR) residues are drawn as yellow bonds. The plug domain TM2a is colored orange. (*B*) The apparent free energy of partitioning $\Delta G(z)$ of an alkyl sidechain (orange) with accessible surface area A_{acc} depends upon position z within the TM segment (solid red curve), because the atomic solvation parameter σ apparently depends upon position. Our results suggest an opposite behavior (dashed orange curve).

explain the magnitudes and position dependence of the translocon/bilayer partitioning solvation parameters? To address this question, we turned to atomistic molecular-dynamics (MD) simulations.

From a number of crystallographic SecY structures (4–8), we chose the SecYE structure from *Pyrococcus furiosus* determined by Egea and Stroud (8), because it appears to be in a nearly open ("primed") state as judged by the separation of the gate helices. We thought at the outset of our simulations that SecYE might close. However, SecYE remained stably open, which allowed close examination of the waters inside SecY. We found that waters deep within the translocon diffuse anomalously, have slow rotational dynamics, and have their dipoles aligned along the SecY axis. These properties indicate that translocons are not simple water-filled pores, which raises fundamental questions about the nature of translocon/bilayer partitioning of TM segments, and more generally about solute partitioning into compartments of restrained water molecules.

Results

SecYE Remained Stably Open During the Simulation. We began our study with a 0.45-μs simulation (Sim1) of SecYE embedded in a palmitoyloleoylphosphatidylcholine (POPC) bilayer in excess water using *NPT* (constant number of particles N, pressure P, and temperature T) conditions (*Methods*). Egea and Stroud (8) reported the *P. furiosus* SecYE translocon structure to be in a primed open state based upon the dimensions of the HR. We monitored the HR radius throughout the simulation (*SI Appendix*, Fig. S1) and found it to be quite stable with a mean radius of 6.8 ±0.3 Å (SD) (see Fig. 3*D*). The same measurement in the closed *Methanococcus jannaschii* SecYEβ yielded 4.6 ± 0.1 Å, as observed by Egea and Stroud (8) (*SI Appendix*, Fig. S2). Consistent with the stability of the ring, the SecY TM region was rather rigid (C_α rmsd < 2 Å; *SI Appendix*, Fig. S4*A*), confirming that SecY did not undergo any major conformational changes during the simulation. We confirmed the stability of the SecY structure by carrying out two additional *NPT* simulations of 130 ns, described in *Supporting Information* (*SI Appendix*, Figs. S4 and S5).

Water Distribution Within SecYE Conforms to the Hourglass Shape of the Interior. To examine the water distribution within SecY, we defined a 40 × 40 × 100-Å^3 square prism ("the prism") enclosing SecY and centered at the simulation cell origin (Fig. 2*B*). The placement resulted in the HR ring being located between $z = \pm 4$ Å (*SI Appendix*, Fig. S1*B*). We then determined the time-averaged number of water molecules within the prism in consecutive slices of 1-Å thickness along the z axis (Fig. 2*C*). The average total number of water molecules within the hourglass between $z = \pm 20$ Å was about 430.

Dewetting phenomena have been observed in MD simulations of hydrophobic protein channels and gates (23–26). We looked for dewetting in the HR region by monitoring the water occupancy within the volume enclosed by the HR sidechains (Fig. 3*A* and *SI Appendix*, Fig. S5). We observed dramatic fluctuations in the number of waters due to lipid acyl chains exploring SecY (Fig. 3 *B* and *C*, and *SI Appendix*, Fig. S3), but there was no evidence of persistent dewetting (Movie S1). The lipids located in front of the gate generally confined the water molecules within SecY (Fig. 3*B* and Movie S2), and they transiently explored the SecY interior, perturbing water passage (Fig. 3*C*, *SI Appendix*, Fig. S3, and Movies S1 and S3). These perturbations took place only after the first 0.15 μs of Sim1 (Fig. 3*A*). To understand how the acyl chains perturbed water within SecY, we examined the time-averaged number of acyl chain carbon atoms inside the prism (*SI Appendix*, Fig. S3*A*). The major acyl chain incursions occur between $z = \pm 10$ Å, but the acyl chain carbon atoms were not able to explore the HR region (*SI Appendix*, Fig. S3*B*) during the first 0.15 μs of Sim1, and only to a limited extent after that time. Because the TM helix insertion process involves direct interactions among lipids, water, translocon, and incoming peptides (11, 16), we suppose that these acyl chains—noted in earlier simulations (27, 28)—are likely to play a role in TM helix insertion. However, we do not know whether the lipids we observed are physiologically significant. Similar incursions were seen in Sim2 and Sim3 (*SI Appendix*, Fig. S5).

Water Dynamics Within the Hourglass Deviates Dramatically from Bulk Behavior. For the analysis of the *NPT* simulations, we stored the system coordinates every 10 ps, but this time interval is too long to reveal the details of water dynamics that occur on the picosecond timescale (29, 30). Therefore, we carried out 40 *NVE* (constant number of particles N, volume V, and energy E) simulations of 50-ps length, saving configurations every 5 fs (*Methods*). Each of the simulations was started from independent initial structures selected from five different time intervals (red horizontal lines, Fig. 3*A*) of Sim1. We determined the translational diffusion and the rotational dynamics of water in the prism enclosing SecY (Fig. 3*B*). We began by examining the first 0.15 μs of Sim1 (dashed vertical red line,

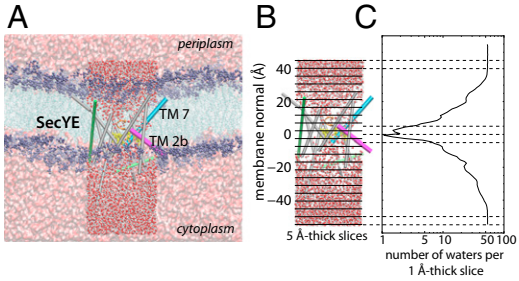

Fig. 2. Water distribution within the SecYE *P. furiosus* translocon. (*A*) Side-view snapshot from the cell of the *P. furiosus* SecYE translocon embedded in a POPC lipid bilayer. The SecY structure and coloring is the same as in Fig. 1*A*. Water molecules inside the 40 × 40 × 100-Å^3 square prism are shown in red (oxygen) and white (hydrogen) van der Waals representation, and those outside in a dimmed surface representation. Periplasmic and cytoplasmic sides of the membrane are indicated. (*B*) Representation of the 20 5-Å-thick slabs (black lines) parallel to the membrane plane used to subdivide the prism for studying water as a function of position along the membrane normal. Coloring is as in *A*. (*C*) Logarithmic representation of water distribution along the membrane normal from the first 0.15 μs of the 0.45-μs Sim1 determined from the time-averaged number of water molecules at 1-Å intervals. The dashed horizontal lines indicate the outermost slabs and the HR location.

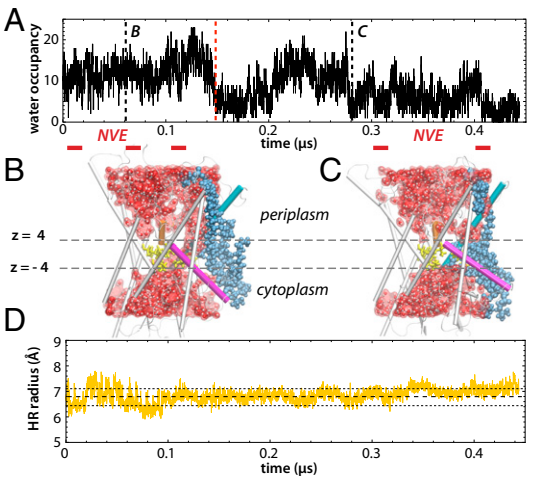

Fig. 3. Fluctuations of water occupancy in the HR region, due in part to incursions of lipid acyl chains. (*A*) Water occupancy calculated over the 0.45-μs simulation in the region enclosing the HR residues. Black dashed lines indicate the times of the snapshots in *B* and *C*; red dashed vertical line defines the time $t = 0.15$ μs at which the lipid acyl chains start exploring the HR region (*SI Appendix*, Fig. S3); red horizontal lines indicate time ranges of *NVE* simulations. (*B* and *C*) Representative snapshots taken at $t = 0.06$ μs (*B*) and $t = 0.28$ μs (*C*). The color scheme is the same as in Fig. 1, except the plug domain TM2a (orange, new cartoon format). Water is represented using both van der Waals and surface representations. Lipids in front of the lateral gate are shown in blue van der Waals format. The gray dashed lines indicate the region explored by the HR residues along the membrane normal (*z* axis). (*D*) Time evolution of the HR radius of SecY. The average value is 6.8 ± 0.3 Å.

Fig. 3*A*), because the water-conducting states within HR were unperturbed by acyl chain incursions (*SI Appendix*, Fig. S3*B*).

We characterized the translational motion of waters by calculating the dependence of mean squared displacements (MSDs) on time (*SI Appendix*, Fig. S6*A*). In general, after a few picoseconds, the MSD became proportional to t^{α} (29). Linear dependence of the MSD on time ($\alpha = 1$) is a signature of Brownian diffusive motion as observed for bulk water; $\alpha < 1$ is a signature of anomalous "subdiffusion," which is characteristic of confined water and protein hydration water. The MSD of water molecules in the long-time regime ($t > 2$ ps) behaved differently in each of the 5-Å-thick slabs, as characterized by α (Fig. 4*A*, solid black circles). Approaching the SecY center, the α decreased from 1 to 0.53, which is similar to values reported for protein hydration water (30–35). The diffusion of water deep within the translocon is therefore anomalous with respect to bulk behavior.

Water dynamics can also be assessed using single-molecule dipole autocorrelation (SDAC) functions $C_{\mu}(t)$, whose decays are determined by local librational and rotational motions of water (*Methods*). We defined the rotational characteristic relaxation time τ_{μ} as the time required for $C_{\mu}(t)$ to decay to $1/e$ to analyze the SDAC functions consistently. The functions exhibited very different trends depending on the location of water within SecY (*SI Appendix*, Fig. S6*B*). Within the 5-Å-thick slabs at the extreme ends of the prism (Fig. 4), a relaxation time $\tau_{\mu} \sim 1$ ps was observed, as expected for bulk water (36) (Fig. 4*B*, *SecY*, solid black circles). Inside SecY, however, τ_{μ} progressively increased to 20–30 ps, due to water–SecY interactions that restricted the reorientational motion of water molecules. Near the center of SecY, water relaxation exceeded the observation time window so that only a lower limit could be determined.

We next performed the same analyses on trajectories obtained from the *NVE* simulations run at times $t > 0.15$ μs, when lipid acyl chains were exploring the interior of SecY. The results revealed an increase in the perturbation of water translational dynamics: α decreased from 1 to 0.40 as the SecY center was approached (Fig. 4*C*). In contrast, lipid incursions influenced water rotational dynamics only weakly (Fig. 4*D*). Approaching the SecY center, the relaxation times are about the same as when water is unperturbed by the lipid acyl chains.

Electrostatic and Confinement Effects Determine Dynamics of Water. What features of SecY cause anomalous water behavior? One possibility is restriction of water movement due to the limited volume of the hourglass (confinement). Another possibility is electrostatic interactions between water and the translocon. We designed two additional 40 *NVE* setups (*Methods*) using the same configurations selected from Sim1. In the first setup, the coordinates of SecY were fixed (*SecY-fix*; *SI Appendix*, Figs. S6 *C* and *D* and S7 *C* and *D*). This approach allowed us to determine the effect of SecY thermal motion on water dynamics. In the second setup (*SecY-vdw*), in addition to "freezing" SecY, we switched off all SecYE charges, including partial charges (*SI Appendix*, Figs. S6 *E* and *F* and S7 *E* and *F*) to separate confinement from electrostatic effects. For $t < 0.15$ μs, water exhibited essentially the same translational dynamics regardless of whether SecY was mobile or frozen (Fig. 4*A*, solid black circles and solid green diamonds, respectively), meaning that the thermal motion of SecYE had little effect on diffusion. However, after switching off electrostatic interactions, water still exhibited anomalous diffusion, but the value of α at the SecY center was 0.72 rather than 0.53 (*SecY-vdw* in Fig. 4*A*). For $t >$ 0.15 μs, when the lipids make incursions inside SecY, α reached 0.63 at the SecY center (*SecY-vdw* in Fig. 4*C*, blue diamonds) instead of 0.40. These findings indicate that both confinement and the SecY electrostatics make water translational dynamics depart from bulk diffusion.

Water rotational dynamics slowed upon freezing SecY (Fig. 4 *B* and *D*; compare black symbols and green diamonds) irrespective of the incursions of the lipid acyl chains inside the SecY pore. We speculate that restraining SecY thermal motions perturbs the

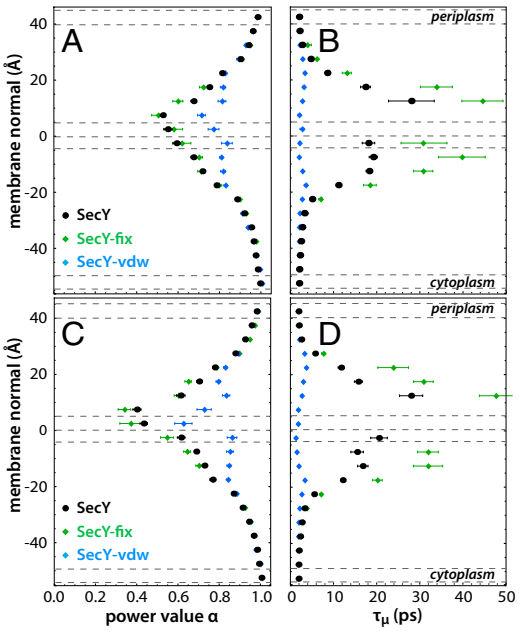

Fig. 4. *NVE* simulations reveal anomalous water motions inside SecY. *A* and *B* show data for $t < 0.15$ μs; *C* and *D* show data for $t > 0.15$ μs. Black circles (*SecY*) show values from unrestrained simulations; green diamonds, those from *SecY-fix*; blue diamonds, those from *SecY-vdw*. (*A* and *C*) Variation of α exponent variation along the membrane normal estimated from the *NVE* simulations. (*B* and *D*) The variation of the rotational relaxation time τ_{μ} along the membrane normal estimated from the *NVE* simulations.

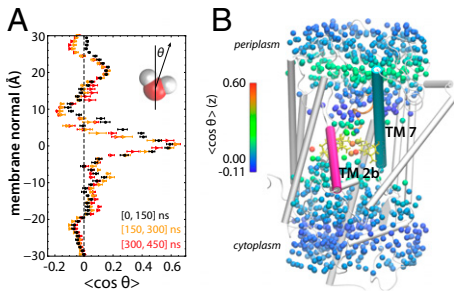

Fig. 5. Water dipoles are aligned near the center of SecY. (*A*) Water dipole orientations were calculated from 0 to 0.15 μs (black symbols), from 0.15 to 0.30 μs (orange symbols), and from 0.30 to 0.45 μs (red symbols) of the *NPT* simulation Sim1 and are shown as a function of position along the membrane normal. (*B*) Representative snapshot of the orientation of the water dipoles within the SecY channel. Water oxygen atoms are drawn as beads and colored according with the value of the order parameter calculated between 0 and 0.15 μs as indicated by the colored bar. SecY is represented using the color scheme of Fig. 1.

rearrangement rate of the SecY hydrogen bond network (37) as well as that of the SecY–water network, thus affecting the water rotational dynamics observed when SecY is mobile (Fig. 4 *B* and *D*; solid black circles labeled *SecY*). Interestingly, once the SecY charges are switched off, water characteristic rotational relaxation times revert to bulk values, typically ∼1 ps, throughout the translocon (Fig. 4 *B*–*D*, solid blue diamonds). Despite the bulk-like relaxation times, the *SecY-vdw* SDAC functions of water molecules located inside SecY differ considerably from those of bulk water (*SI Appendix*, Figs. S6*F* and S7*F*), which indicates that water inside SecY in the absence of the electrostatic field behaves differently from bulk water.

Water Molecules Are Highly Oriented Inside the SecYE Translocon. The simplest way to examine the effect of the SecY electrostatics on water structure and the interpretation of the relaxation time τ_μ in the absence of charges is to determine the average orientation of water dipoles with respect to the SecY *z* axis using the order parameter $P_d\ (z) = \langle\cos\theta\rangle(z)$ (*Methods*). A random distribution of dipole moments corresponds to $P_d\ (z) = 0$. We first analyzed Sim1 and calculated the distribution of the water dipole orientation over three time windows: 0–0.15 μs, 0.15–0.3 μs, and 0.3–0.45 μs. Our analysis of P_d is displayed in Fig. 5 along with a representative snapshot in which water oxygen atoms are colored according to the dipole orientation calculated between 0 and 0.15 μs. These results show that water exhibits nearly the same behavior over the whole length of Sim1. Outside SecY, water dipoles do not show any net orientational preference. Within SecY P_d varies between −0.2 and 0.6, with the strongest orientation $\langle\cos\theta\rangle = 0.6$ occurring near the hydrophobic ring. This result reflects a very high degree of alignment, and explains the trends observed for the *SecY* SDAC functions in this region (*SI Appendix*, Figs. S6*B* and S7*B*). The lack of $C_\mu(t)$ decay within the time window studied is a signature of an almost fixed dipole direction.

The dipole alignment observed is comparable with that exhibited by water in the aquaporin channel (38) or in a mechanosensitive channel (39). To clarify whether or not the alignment was due to electrostatics or confinement, we calculated the average orientation of the water dipoles for all of the 120 *NVE* simulations, including *SecY-fix* and *SecY-vdw* (*SI Appendix*, Fig. S8 *A* and *C*). When the SecY charges were turned off (*SecY-vdw*, blue symbols), the water dipoles were still aligned to the membrane normal, but less than observed in the *SecY* simulations (*SI Appendix*, Fig. S8 *A* and *C*, compare blue and black symbols). This observation agrees with the distinct, non–bulk-like evolution of the *SecY-vdw* SDAC functions (*SI Appendix*, Figs. S6*F* and S7*F*), despite the significantly decreased decay times. We thus conclude that both the SecY electrostatics and the confinement affect the water behavior. Moreover, the presence of lipid acyl chains within the SecY pore further affects the intensity and direction of the dipole alignment (*SI Appendix*, Fig. S8 *C* and *D*).

Discussion

Our simulations bear strongly on the interplay between the translocon and the lipids. During our 0.45-μs simulation, the hydrophobic pore ring remained stably open independent of lipid intrusions (Fig. 3*D*). These results suggest that the primed open configuration of SecYE may represent a stable conformational state on the timescale of our simulation. The involvement of the lipids in the nascent-chain integration process has been suggested in previous experimental (11, 40) and computational (27, 28) studies. Our simulations provide evidence for the accessibility of the SecY pore to lipid chains of the surrounding bilayer, supporting the possibility of direct peptide-lipid interactions.

The main finding of our simulations is that water inside SecY does not behave as in bulk: translational diffusion deviates markedly from Brownian motion (Fig. 4 *A* and *C*) and the rotational dynamics show strong retardation (Fig. 4 *B* and *D*). These features are typical for water in confined environments and at hydrated protein surfaces (32, 33, 41, 42). Moreover, and perhaps more important for the thermodynamics of partitioning TM segments into the membrane, we observe that water dipoles in the HR region ($z = \pm 4$ Å; *SI Appendix*, Fig. S1*B*) are oriented preferentially parallel to the pore axis pointing toward the exterior (Fig. 5). The inhomogeneous nonbulk properties of water within SecY suggest that translocon/membrane partitioning cannot be compared directly to partitioning between bulk aqueous and lipid phases. Contrary to expectations formed in the days when the structures of only a few membrane proteins were known, we now know that the interiors of membrane proteins (43–47), and even soluble proteins (48, 49), can contain considerable amounts of water, which raises the question of how restricted waters might participate in or affect protein function.

Our results reveal the importance of the SecY electrostatics, which might explain, for example, why flanking charges in model TM segments affect insertion by the Sec61 translocon (50). Moreover, the dipole alignment of water molecules within SecY might be a signature of another potential role of water in the membrane insertion process. For instance, it has been shown that water can facilitate or screen the interactions between lipids and a peptide located inside SecY (15). Furthermore, the dipole alignment could be crucial for the interaction of the positively charged N terminus of a signal sequence with the translocon and consequentially for membrane protein topology. The presence of a highly polarizing field will likely affect helix insertion. If the idea that incoming peptides pass directly through the SecY hourglass is correct, they would likely replace a substantial number of water molecules in the translocon interior. Hence, they would be exposed to an electrostatic field comparable to that experienced by the water molecules in our simulations. A dipole orientation that mimics these aligned water dipoles could therefore have a substantial stabilizing effect.

Favorable water-to-hydrocarbon partitioning free energies of hydrophobic moieties observed in bulk partitioning arise, in part, from the release of oriented water molecules at hydrophobic residue surfaces (51). Given a hydrophobic α-helix inside the SecY translocon that simply partitions parallel to the membrane plane into the bilayer (Fig. 1*B*), one would expect the solvation parameter σ for hydrophobic amino acids at the ends of the helix to be similar to bulk values, because water at the extreme ends of the translocon is bulk-like. Öjemalm et al. (22) observed, however, σ at the helix ends was −6 kcal·mol^{-1}·Å^{-2}, which is about one-fourth of the value expected for partitioning from bulk water. Given that water is restrained at the center of the translocon, what value of σ would one expect for amino acids at the center of a hydrophobic α-helix? To

answer that question, other questions must be answered. Is water present inside SecY when a helix is present? If water is present and restrained due to SecY electrostatics and confinement, how is σ affected? If water is absent, what is the meaning of σ? One scenario might be that amino acids located in the center of a helix in the translocon have neighboring oriented water molecules that remain ordered even after the helix moves into the bilayer. In that case, the apparent solvation parameter at the helix center should be less favorable than at the helix ends. Thus, in experiments such as those of Öjemalm et al. (22), one might expect solvation parameters to be least favorable near the helix center and most favorable near the helix ends (dashed orange curve, Fig. 1*B*), which is exactly opposite to the results of Öjemalm et al. (solid red line, Fig. 1*B*). This contradiction raises fundamental questions about the translocon/membrane partitioning process of TM helices. Cymer et al. (52) have suggested that nascent TM helices may preferentially interact with the gate helices and the membrane interface (53, 54) without first passing through the SecY hourglass.

Finally, the crucial question our results raise is whether the concept of hydrophobic effect-driven partitioning even applies when a nonpolar solute moves from a restrained water region into the water-free bilayer interior. Or more simply and fundamentally, what is the partitioning free energy of solutes between water in bulk and water in restraining confined spaces? Although much theoretical and experimental work has been devoted to describing the properties of water in bulk (55) and in confined spaces (56) such as inverted micelles (57), this fundamental question remains unanswered as far as we can establish.

Methods

MD Simulations in the *NPT* Ensemble. The atomic coordinates of the SecYE translocon were extracted from the *Pyrococcus furiosus* crystal structure (8) [Protein Data Bank (PDB) ID code 3MP7]. From this structure, we set up and carried out three independent *NPT* simulations: Sim1, Sim2, and Sim3 (*SI Appendix*, Table S1). In all cases, we embedded SecYE in a POPC bilayer formed by 600 lipids (300 molecules each leaflet). The protocols we used to model residues missing in the original structure, to embed the completed SecYE structure in the POPC lipid bilayer, and to minimize and equilibrate the systems are reported in *Supporting Information*. We also carried out MD simulations using the *M. jannaschii* SecYEβ translocon crystal structure (4) (PDB ID code 1RHZ). The same protocols were followed as for *P. furiosus* SecYE.

We used NAMD (58, 59), version 2.9, with the CHARMM36 (60) force field for the lipids and the CHARMM22 force field with the CMAP correction for the protein and ions (61, 62). The TIP3P model (63) was used for water molecules. The temperature was kept constant at 300 K using a Langevin dynamics scheme, and the pressure was maintained constant at 1 atm using anisotropic coupling in conjunction with Nosé–Hoover–Langevin piston algorithm (64, 65). Periodic boundary conditions were applied in three dimensions. The electrostatic interactions were computed by means of the smooth particle-mesh Ewald summation method (66, 67) and the short-range real-space interactions were cut off at 12 Å using a switching function between 10 and 12 Å. The equations of motion were integrated with a time step of 4 fs for the long-range electrostatic forces, 2 fs for the short-range nonbonded forces, and 1 fs for the bonded forces by means of a multiple-time step algorithm (68). The SHAKE (69) algorithm was used to constrain the length of the bonds involving hydrogen atoms. Coordinates were saved every 10 ps.

MD Simulations in the *NVE* Ensemble from Sim1. To characterize water properties within SecY and to investigate how the SecY pore affects water dynamics, we performed five sets of eight *NVE* simulations, i.e., 40 *NVE* simulations in total. We selected the eight independent configurations every 2 ns from the following five time ranges of Sim1: 2–16, 60–74, 104–118, 302–316, and 402–416 ns. We used these 40 structures as starting configurations for running *NVE* simulations of 50-ps length. To have high resolution in time, we collected coordinates every 5 fs.

In addition to these five sets of eight *NVE* simulations in which the protein complex was unrestrained (labeled *SecY* in Fig. 4), we used the same starting structures to carry out two more groups of five sets of eight *NVE* simulations, applying restraints as follows. In the first group, we applied harmonic restraints to freeze SecY (labeled *SecY-fix* in Fig. 4), and in the second, in addition to freezing SecY, we switched the SecY–water electrostatic interactions off by setting the protein atom charges to zero (labeled *SecY-vdw* in Fig. 4). These three groups of 40 *NVE* simulations (*SecY*, *SecY-fix*, and *SecY-vdw*) enabled us to examine how the cavity shape and the electrostatics of SecY affect individually the dynamics of water. In total, we generated and analyzed 120 *NVE* simulations, summarized in *SI Appendix*, Table S2.

Water Anomalous Dynamics. We investigated water dynamics in a selected region of the simulation cell characterized by a volume of 40 × 40 × 100-Å^3 encompassing SecY (Fig. 2*B*). We subsequently divided this square prism into 20 5-Å-thick slabs parallel to the membrane (Fig. 2*C*). For each slab, we first computed and analyzed the MSDs, which characterize the translational diffusion of water molecules. MSDs are defined as follows:

$$MSD(t) = \langle |\bar{r}_i(t) - \bar{r}_i(0)|^2 \rangle,$$

where $\bar{r}_i(t)$ denotes the position of the particle i at time t, and the brackets denote an average over molecules and time origins. In *SI Appendix*, Figs. S6 *A*, *C*, and *E*, and S7 *A*, *C*, and *E*, we present the MSD of the center of mass of water molecules computed for the *SecY*, *SecY-fix*, and *SecY-vdw* for each slab and for times $t < 0.15$ μs and $t > 0.15$ μs. In the long-time regime, the time dependence of the MSD can be described with a power law $MSD(t) = kt^{\alpha}$, and the α exponent gives information on the diffusive character of water motion. We fitted the MSD to the power-law function for $t > 2$ ps and represented the α values in Fig. 4. Further details of the protocol used for the data analysis are reported in *Supporting Information*.

Subsequently, we calculated the SDAC functions $C_\mu(t)$, which signify the rotational motion of water molecules and are defined as follows:

$$C_\mu(t) = \frac{\langle \hat{\mu}(t) \cdot \hat{\mu}(0) \rangle}{\langle \hat{\mu}(0) \cdot \hat{\mu}(0) \rangle},$$

where $\hat{\mu}(t)$ is the unit vector of the water dipole at time t. In *SI Appendix*, Figs. S6 *B*, *D*, and *F*, and S7 *B*, *D*, and *F*, we have plotted the SDAC functions computed for *SecY*, *SecY-fix*, and *SecY-vdw* for each slab for the time windows $t < 0.15$ μs and $t > 0.15$ μs. We analyzed consistently all of the 120 *NVE* simulations and calculated the characteristic relaxation time τ_μ as the time at which $C_\mu(t)$ decays to 1/*e*, that is, $C_\mu(\tau_\mu) = 1/e$ (*SI Appendix*, Figs. S6 and S7, dashed lines). The τ_μ values are reported in Fig. 3. Further details of the data analysis procedure are reported in *Supporting Information*.

Finally, we examined the water dipole orientation within the SecY channel in terms of the water orientational order parameter defined as follows:

$$P_d(z) = \langle \cos\theta \rangle(z),$$

where θ is the angle between the water dipole and the membrane normal. The θ value varies between 0° and 180°, hence $\cos\theta$ varies between −1 and 1. We calculated the values of $\cos\theta$ between 0 and 0.15 μs, 0.15 and 0.3 μs, and 0.3 and 0.45 μs of Sim1 (Fig. 5), and over all of the *NVE* simulations (*SecY*, *SecY-fix*, and *SecY-vdw*) (*SI Appendix*, Fig. S8 *A* and *C*). The procedure we followed is described in detail in *Supporting Information*.

ACKNOWLEDGMENTS. We thank J. Alfredo Freites for extremely valuable discussions and Joseph Farran for excellent technical support. We thank Prof. Kim Sharp for useful discussions of restrained waters in proteins. A.-N.B. and S.C. thank the International Office of the Freie Universität, Berlin, for travel support. This research was supported by National Institutes of Health Grants R01 GM74637 (to S.H.W.) and P01 GM86685 (to D.J.T. and S.H.W.). M.H. was supported by the German National Academy of Science, Leopoldina. A.-N.B. was supported in part by Marie Curie International Reintegration Award IRG 276920. The simulations were performed in part on the High-Performance Computing Cluster at the University of California, Irvine, and in part on Stampede on Extreme Science and Engineering Discovery Environment, supported by National Science Foundation Grant ACI-1053575.

1. Osborne AR, Rapoport TA, van den Berg B (2005) Protein translocation by the Sec61/SecY channel. *Annu Rev Cell Dev Biol* 21:529–550.
2. White SH, von Heijne G (2008) How translocons select transmembrane helices. *Annu Rev Biophys* 37:23–42.
3. Denks K, et al. (2014) The Sec translocon mediated protein transport in prokaryotes and eukaryotes. *Mol Membr Biol* 31(2-3):58–84.
4. Van den Berg B, et al. (2004) X-ray structure of a protein-conducting channel. *Nature* 427(6969):36–44.
5. Zimmer J, Nam Y, Rapoport TA (2008) Structure of a complex of the ATPase SecA and the protein-translocation channel. *Nature* 455(7215):936–943.
6. Tsukazaki T, et al. (2008) Conformational transition of Sec machinery inferred from bacterial SecYE structures. *Nature* 455(7215):988–991.

7. Frauenfeld J, et al. (2011) Cryo-EM structure of the ribosome-SecYE complex in the membrane environment. *Nat Struct Mol Biol* 18(5):614–621.
8. Egea PF, Stroud RM (2010) Lateral opening of a translocon upon entry of protein suggests the mechanism of insertion into membranes. *Proc Natl Acad Sci USA* 107(40): 17182–17187.
9. du Plessis DJF, Berrelkamp G, Nouwen N, Driessen AJM (2009) The lateral gate of SecYEG opens during protein translocation. *J Biol Chem* 284(23):15805–15814.
10. Hizlan D, et al. (2012) Structure of the SecY complex unlocked by a preprotein mimic. *Cell Rep* 1(1):21–28.
11. Heinrich SU, Mothes W, Brunner J, Rapoport TA (2000) The Sec61p complex mediates the integration of a membrane protein by allowing lipid partitioning of the transmembrane domain. *Cell* 102(2):233–244.
12. Gumbart J, Chipot C, Schulten K (2011) Free-energy cost for translocon-assisted insertion of membrane proteins. *Proc Natl Acad Sci USA* 108(9):3596–3601.
13. Zhang B, Miller TF, 3rd (2010) Hydrophobically stabilized open state for the lateral gate of the Sec translocon. *Proc Natl Acad Sci USA* 107(12):5399–5404.
14. Rychkova A, Vicatos S, Warshel A (2010) On the energetics of translocon-assisted insertion of charged transmembrane helices into membranes. *Proc Natl Acad Sci USA* 107(41):17598–17603.
15. Zhang B, Miller TF, 3rd (2012) Direct simulation of early-stage Sec-facilitated protein translocation. *J Am Chem Soc* 134(33):13700–13707.
16. Hessa T, et al. (2005) Recognition of transmembrane helices by the endoplasmic reticulum translocon. *Nature* 433(7024):377–381.
17. Hessa T, et al. (2007) Molecular code for transmembrane-helix recognition by the Sec61 translocon. *Nature* 450(7172):1026–1030.
18. White SH, Wimley WC (1999) Membrane protein folding and stability: Physical principles. *Annu Rev Biophys Biomol Struct* 28:319–365.
19. Tanford C (1973) *The Hydrophobic Effect: Formation of Micelles and Biological Membranes* (Wiley, New York), 1st Ed.
20. Reynolds JA, Gilbert DB, Tanford C (1974) Empirical correlation between hydrophobic free energy and aqueous cavity surface area. *Proc Natl Acad Sci USA* 71(8):2925–2927.
21. Wimley WC, Creamer TP, White SH (1996) Solvation energies of amino acid side chains and backbone in a family of host-guest pentapeptides. *Biochemistry* 35(16): 5109–5124.
22. Öjemalm K, et al. (2011) Apolar surface area determines the efficiency of translocon-mediated membrane-protein integration into the endoplasmic reticulum. *Proc Natl Acad Sci USA* 108(31):E359–E364.
23. Zhu F, Hummer G (2010) Pore opening and closing of a pentameric ligand-gated ion channel. *Proc Natl Acad Sci USA* 107(46):19814–19819.
24. Anishkin A, Sukharev S (2004) Water dynamics and dewetting transitions in the small mechanosensitive channel MscS. *Biophys J* 86(5):2883–2895.
25. Beckstein O, Sansom MSP (2006) A hydrophobic gate in an ion channel: The closed state of the nicotinic acetylcholine receptor. *Phys Biol* 3(2):147–159.
26. Jensen MØ, et al. (2010) Principles of conduction and hydrophobic gating in K^+ channels. *Proc Natl Acad Sci USA* 107(13):5833–5838.
27. Gumbart J, Schulten K (2007) Structural determinants of lateral gate opening in the protein translocon. *Biochemistry* 46(39):11147–11157.
28. Gumbart JC, Teo I, Roux B, Schulten K (2013) Reconciling the roles of kinetic and thermodynamic factors in membrane-protein insertion. *J Am Chem Soc* 135(6): 2291–2297.
29. Bizzarri AR, Rocchi C, Cannistraro S (1996) Origin of the anomalous diffusion observed by MD simulation at the protein-water interface. *Chem Phys Lett* 263(3-4):559–566.
30. Pizzitutti F, Marchi M, Sterpone F, Rossky PJ (2007) How protein surfaces induce anomalous dynamics of hydration water. *J Phys Chem B* 111(26):7584–7590.
31. Settles M, Doster W (1996) Anomalous diffusion of adsorbed water: A neutron scattering study of hydrated myoglobin. *Faraday Discuss* 103:269–279.
32. Marchi M, Sterpone F, Ceccarelli M (2002) Water rotational relaxation and diffusion in hydrated lysozyme. *J Am Chem Soc* 124(23):6787–6791.
33. Choudhury N, Pettitt BM (2005) Dynamics of water trapped between hydrophobic solutes. *J Phys Chem B* 109(13):6422–6429.
34. Tobias DJ, Kuo IW, Razmara A, Tarek M (2003) Protein hydration in water. *Water in Confining Geometries*, eds Devlin JP, Buch V (Springer, Berlin), pp 213–310.
35. Sengupta N, Jaud S, Tobias DJ (2008) Hydration dynamics in a partially denatured ensemble of the globular protein human α-lactalbumin investigated with molecular dynamics simulations. *Biophys J* 95(11):5257–5267.
36. Pal S, Bandyopadhyay S (2013) Importance of protein conformational motions and electrostatic anchoring sites on the dynamics and hydrogen bond properties of hydration water. *Langmuir* 29(4):1162–1173.
37. Bondar A-N, del Val C, Freites JA, Tobias DJ, White SH (2010) Dynamics of SecY translocons with translocation-defective mutations. *Structure* 18(7):847–857.
38. Tajkhorshid E, et al. (2002) Control of the selectivity of the aquaporin water channel family by global orientational tuning. *Science* 296(5567):525–530.
39. Spronk SA, Elmore DE, Dougherty DA (2006) Voltage-dependent hydration and conduction properties of the hydrophobic pore of the mechanosensitive channel of small conductance. *Biophys J* 90(10):3555–3569.
40. Duong F, Wickner W (1998) Sec-dependent membrane protein biogenesis: SecYEG, preprotein hydrophobicity and translocation kinetics control the stop-transfer function. *EMBO J* 17(3):696–705.
41. Moilanen DE, Levinger NE, Spry DB, Fayer MD (2007) Confinement or the nature of the interface? Dynamics of nanoscopic water. *J Am Chem Soc* 129(46):14311–14318.
42. Laage D, Stirnemann G, Sterpone F, Rey R, Hynes JT (2011) Reorientation and allied dynamics in water and aqueous solutions. *Annu Rev Phys Chem* 62:395–416.
43. Pebay-Peyroula E, et al. (2003) Structure of mitochondrial ADP/ATP carrier in complex with carboxyatractyloside. *Nature* 426(6962):39–44.
44. Pryor EE, Jr, et al. (2013) Structure of the integral membrane protein CAAX protease Ste24p. *Science* 339(6127):1600–1604.
45. Quigley A, et al. (2013) The structural basis of ZMPSTE24-dependent laminopathies. *Science* 339(6127):1604–1607.
46. Manolaridis I, et al. (2013) Mechanism of farnesylated CAAX protein processing by the intramembrane protease Rce1. *Nature* 504(7479):301–305.
47. Abramson J, et al. (2003) Structure and mechanism of the lactose permease of *Escherichia coli*. *Science* 301(5633):610–615.
48. Miles EW, Rhee S, Davies DR (1999) The molecular basis of substrate channeling. *J Biol Chem* 274(18):12193–12196.
49. Sun T, Lin F-H, Campbell RL, Allingham JS, Davies PL (2014) An antifreeze protein folds with an interior network of more than 400 semi-clathrate waters. *Science* 343(6172):795–798.
50. Lerch-Bader M, Lundin C, Kim H, Nilsson I, von Heijne G (2008) Contribution of positively charged flanking residues to the insertion of transmembrane helices into the endoplasmic reticulum. *Proc Natl Acad Sci USA* 105(11):4127–4132.
51. Madan B, Sharp K (1999) Changes in water structure induced by a hydrophobic solute probed by simulation of the water hydrogen bond angle and radial distribution functions. *Biophys Chem* 78(1-2):33–41.
52. Cymer F, von Heijne G, White SH (2015) Mechanisms of integral membrane protein insertion and folding. *J Mol Biol* 427(5):999–1022.
53. Ulmschneider MB, et al. (2014) Spontaneous transmembrane helix insertion thermodynamically mimics translocon-guided insertion. *Nat Commun* 5:4863.
54. Wimley WC, White SH (1996) Experimentally determined hydrophobicity scale for proteins at membrane interfaces. *Nat Struct Biol* 3(10):842–848.
55. Chandler D (2005) Interfaces and the driving force of hydrophobic assembly. *Nature* 437(7059):640–647.
56. Rasaiah JC, Garde S, Hummer G (2008) Water in nonpolar confinement: From nanotubes to proteins and beyond. *Annu Rev Phys Chem* 59:713–740.
57. Levinger NE (2002) Chemistry. Water in confinement. *Science* 298(5599):1722–1723.
58. Kalé L, et al. (1999) NAMD2: Greater scalability for parallel molecular dynamics. *J Comput Phys* 151(1):283–312.
59. Phillips JC, et al. (2005) Scalable molecular dynamics with NAMD. *J Comput Chem* 26(16):1781–1802.
60. Klauda JB, et al. (2010) Update of the CHARMM all-atom additive force field for lipids: Validation on six lipid types. *J Phys Chem B* 114(23):7830–7843.
61. MacKerell AD, Jr, et al. (1998) All-atom empirical potential for molecular modeling and dynamics studies of proteins. *J Phys Chem B* 102(18):3586–3616.
62. MacKerell AD, Jr, Feig M, Brooks CL, 3rd (2004) Extending the treatment of backbone energetics in protein force fields: Limitations of gas-phase quantum mechanics in reproducing protein conformational distributions in molecular dynamics simulations. *J Comput Chem* 25(11):1400–1415.
63. Jorgensen WL, Chandrasekhar J, Madura JD, Impey RW, Klein ML (1983) Comparison of simple potential functions for simulating liquid water. *J Chem Phys* 79(2):926–935.
64. Martyna GJ, Tobias DJ, Klein ML (1994) Constant-pressure molecular-dynamics algorithms. *J Chem Phys* 101(5):4177–4189.
65. Feller SE, Zhang Y, Pastor RW, Brooks BR (1995) Constant pressure molecular dynamics simulation: The Langevin piston method. *J Chem Phys* 103(11):4613–4621.
66. Darden T, York D, Pedersen L (1993) Particle mesh Ewald: An $N\bullet\log(N)$ method for Ewald sums in large systems. *J Chem Phys* 98(12):10089–10092.
67. Essmann U, et al. (1995) A smooth particle mesh Ewald method. *J Chem Phys* 103(19): 8577–8593.
68. Grubmüller H, Heller H, Windemuth A, Schulten K (1991) Generalized Verlet algorithm for efficient molecular dynamics simulations with long-range interactions. *Mol Simul* 6(1-3):121–142.
69. Ryckaert J-P, Ciccotti G, Berendsen HJC (1977) Numerical integration of the Cartesian equations of motion of a system with constraints: Molecular dynamics of *n*-alkanes. *J Comput Phys* 23(3):327–341.

Supporting Information

Capponi et al. 10.1073/pnas.1424483112

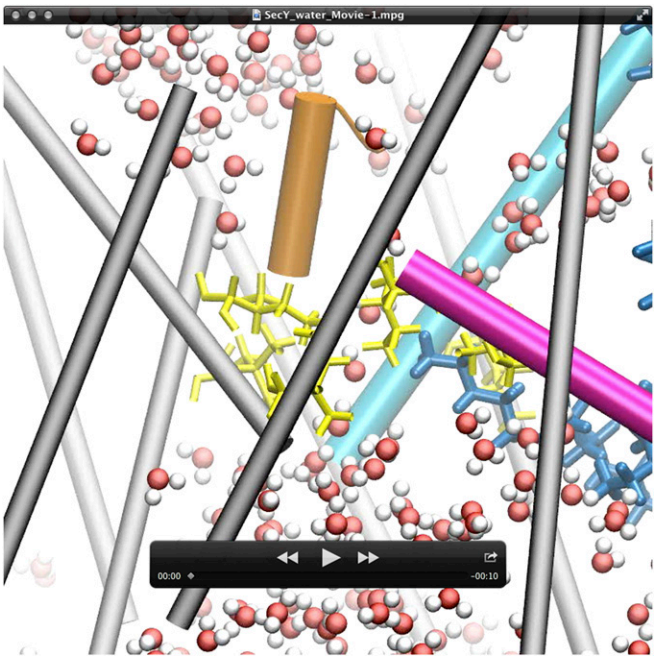

Movie S1. Passage of water molecules through the translocon of *Pyrococcus furiosus*. The movie is derived from the water movement captured in Sim1. The movie shows 1.5 ns of the simulation starting at the 276.8-ns point of Sim1. Shown here is the first frame of the movie.

Movie S1

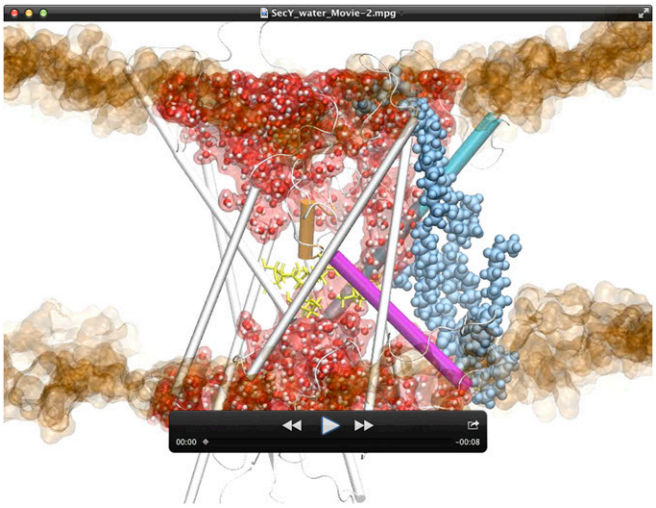

Movie S2. Images of lipids at the front of the lateral gate of SecYE and not interfering with water movement in the vicinity of the hydrophobic ring. The movie shows the structure of SecYE and the lipids as SecYE is rotated about the *z* axis. The movie is essentially a rotating view of Fig. 3*B*. Shown here is the first frame of the movie.

Movie S2

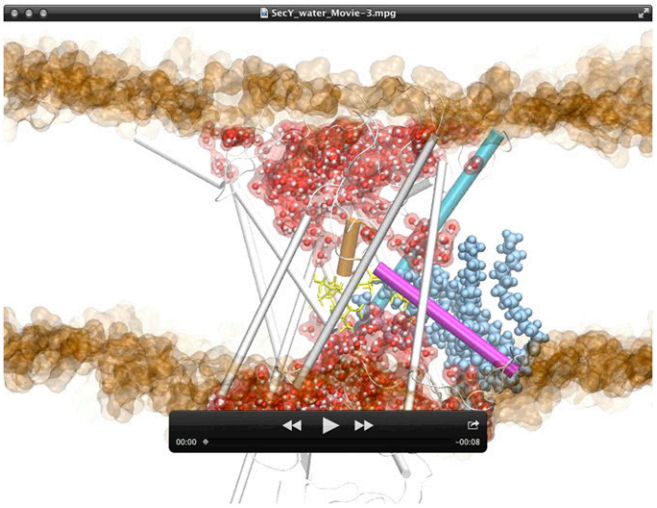

Movie S3. Images of lipids with acyl chains dipping into SecYE and interfering with water movement in the vicinity of the hydrophobic ring. The movie shows the structure of SecYE and the lipids as SecYE is rotated about the *z* axis. The movie is essentially a rotating view of Fig. 3*C*. Shown here is the first frame of the movie.

Movie S3

Other Supporting Information Files

SI Appendix (PDF)

Supplementary Information

Anomalous behavior of water inside the SecY translocon

Sara Capponi[a], Matthias Heyden[b,1], Ana-Nicoleta Bondar[c], Douglas J. Tobias,[b] and Stephen H. White[a,2]

[a]Department of Physiology and Biophysics and Center for Biomembrane Systems, University of California at Irvine, Irvine, California 92697-4560

[b]Department of Chemistry and Center for Biomembrane Systems, University of California at Irvine, Irvine, California, USA 92697-2025

[c]Department of Physics, Freie Universität Berlin, 14195 Berlin-Dahlem, Germany

[1]Current address: Theoretical Chemistry, Max-Planck-Institut fur Kohlenforschung, Mulheim an der Ruhr, Germany

Supplementary Methods and Results

MD simulations in the NPT ensemble. A number of residues from the *Pyrococcus furiosus* crystal structure (1) (Protein Data Bank code 3MP7) primarily in the helix connecting links, were unresolved. We modeled these into the structure using Phyre2 software (2). The completed SecYE structure was subsequently energy minimized in vacuum, and this minimized conformation was used for setting up three independent simulations: Sim1, Sim2, and Sim3 (See Table S1). In all cases, we embedded SecYE in a POPC bilayer formed by 600 lipids (300 molecules each leaflet). Using the VMD software (3), we aligned the principal axes of SecY along the *x*, *y* and *z* directions (*z*-axis normal to the bilayer). The final position of the protein complex within the lipid bilayer was achieved by placing the SecE amphiphilic helix in the membrane interface, avoiding hydrophobic mismatch. The system was then solvated by water molecules, and chloride ions were added to maintain charge neutrality. Several lipid and water molecules were removed to avoid steric clashes. The whole system was relaxed by energy minimization using the conjugate gradient algorithm for 10,000 steps and gradually heated from 25 K to 300 K. Sim1, Sim2, and Sim3 were initiated from the same minimized configuration but using different random initial velocities. Compared with Sim1, in Sim3 (Fig. S4C, Fig. S5B), we also repeated the whole set up protocol described above 'from scratch', i. e. from embedding the SecYE complex in a POPC bilayer. The procedure for equilibrating the system is described in the following.

System Equilibration Protocol. In order to equilibrate the positions of lipids, ions, water molecules, and protein complex, harmonic restraints were used in a series of five consecutive simulation runs of 1 ns, as follows. In the first equilibration run, restraint force constants of 5 kcal mol^{-1} $Å^{-2}$ were applied to the protein backbone atoms and 0.5 kcal mol^{-1} $Å^{-2}$ to ions, water, and lipid headgroups located farther than ~ 10 Å from the protein. In the subsequent two runs, the restraints on the protein backbone were decreased to 2 and then to 1 kcal mol^{-1} $Å^{-2}$, while restraints on ions, water, and lipid headgroups were 0.2 and to 0 kcal mol^{-1} $Å^{-2}$, respectively. After the last 1 ns equilibration run, in which the restraints on the protein backbone were set to 0.5 kcal mol^{-1} $Å^{-2}$ while the rest of the system was unrestrained, we carried out a further 1 ns run with all the restraints removed. We then began the production runs. The simulations were carried out under *NPT* conditions (constant number of particles *N*, pressure *P*, and temperature *T*). We also carried out MD simulations using the *M. jannaschii* SecYEβ translocon crystal structure (4) (PDB code 1RHZ). The same protocols were followed as for *P. furiosus* SecYE.

Dynamics of the 'primed' translocon in a POPC bilayer from Sim2 and Sim3. As we observed in Sim1, SecY remained in the primed open state throughout the whole length of Sim2 (Fig. S4B

and S5A) and Sim3 (Fig. S4C and S5B). Although portions of the lipid acyl chains made incursions into the water-filled interior of SecY, the HR radius was unaffected by the incursions. In all of the simulations, the SecY TM region was rigid with C_α RMSD fluctuating around 2 Å (Fig. S4), and the acyl chains of several lipids—initially located in front of the lateral gate—explored the SecY interior, sometimes perturbing the water occupation (Fig. 3, Fig. S3 and Fig. S5). In Sim2 and Sim3, we detected interruptions in the water permeation through SecY after tens of ns, and in Sim1 after 0.16 μs. Sim1 was thus prolonged for 0.45 μs and 40 independent configurations were used to initiate the *NVE* simulations described in the next section.

MD simulations in the NVE ensemble from Sim1. In order to characterize water properties within SecY, we performed 5 sets of 8 *NVE* (constant number of particles *N*, volume *V* and energy *E*) simulations, i.e. 40 *NVE* simulations in total. We selected the 8 independent configurations every 2 ns from the following 5 time ranges of Sim1: 2 to 16 ns, 60 to 74 ns, 104 to 118 ns, 302 to 316 ns, and 402 to 416 ns. In addition to these 40 *NVE* simulations, we carried out a group of 40 *NVE* simulations in which SecY was maintained fixed (labeled *SecY-fix* in Fig. 4) and another group of 40 *NVE* simulations, in which we fixed SecY and switched the SecY-water electrostatic interactions off by setting the protein atom charges to zero (labeled *SecY-vdw* in Fig. 4). These 3 groups of 40 *NVE* simulations summarized in Table S2 enabled us to examine how the cavity shape and the electrostatics of SecY affect individually the dynamics of water. For the results presented in Figure 4, we grouped together the 3 sets of 8 *NVE* simulations carried out in the time windows $t < 0.15$ μs and the 2 carried out in the time windows $t > 0.15$ μs (see dashed red line Fig. 3A), we analyzed the data and averaged the results.

Water anomalous dynamics from the NVE simulations: translational diffusion. We studied water translational diffusion by computing the mean squared displacements (MSD) of the center-of-mass of the water molecules. We calculated the MSD for each slab and for the *SecY*, *SecY-fix* and *SecY-vdw* simulations and we represented the average of the *NVE* runs from times $t < 0.15$ μs and $t > 0.15$ μs in the left-hand panels of Fig. S6 and S7, respectively. Colored lines describe water inside SecY and black lines those outside SecY (bulk water). In the long-time regime, the time dependence of the MSD can be described with a power law function $MSD(t) = kt^{\alpha}$ (5, 6). The α exponent gives information on the diffusive character of water motion; the constant *k* is a fitting parameter whose value is irrelevant in the present study. A linear dependence on time ($\alpha = 1$) of the MSD is a signature of Brownian motion exhibited by bulk water molecules. A MSD sublinear time-dependence ($\alpha < 1$) indicates anomalous diffusion, which is characteristic of protein hydration water and of confined water. We used the same procedure to analyze all the 120 *NVE* simulations. We fitted the MSD to the power law function

for t > 2 ps and we estimated the value of the α exponent for each slab and each *NVE* run. We averaged the results obtained from *NVE* simulations starting from system configurations sampled from Sim1 at times t < 0.15 μs and times t > 0.15 μs. The results are presented in Fig. 4A-C with the corresponding standard errors.

Water anomalous dynamics from the NVE simulations: rotational dynamics. The $C_\mu(t)$ functions reflect the combination of several dynamical processes taking place at different time windows and their decay is usually described by a sum of exponential or stretched exponential functions, whose amplitudes, parameters, and characteristic relaxation times are related to the type of motion involved. We defined the characteristic relaxation time τ_μ as the time at which $C_\mu(t)$ decays to 1/e, that is $C_\mu(\tau_\mu) = 1/e$. This definition enabled us to analyze all of the slabs and all of the 120 *NVE* simulations consistently. In the right-hand panels of Figure S6 and S7, we represented the SDAC functions computed for *SecY*, *SecY-fix,* and *SecY-vdw* for each slab and averaged for *NVE* simulations starting at times t < 0.15 μs and t > 0.15 μs. The dashed lines represent 1/e. Colored lines describe water inside SecY and black lines water outside SecY, which correspond to bulk water. We first analyzed individually each slab and each set of *NVE* simulations and estimated the value of τ_μ. Subsequently, we grouped the results obtained from the *NVE* runs starting at time t < 0.15 μs and t > 0.15 μs. The results are shown in Fig. 4B-D with the corresponding standard errors. In the *SecY* and *SecY-fix* simulations, the SDAC functions of the water molecules located between −20 Å and +20 Å did not decay. Therefore, we fitted them with a 3-exponential function and extrapolated them to 1/*e* to determine estimates of τ_μ. Because of the lack of decay of the *SecY* and the *SecY-fix* SDAC functions between -5 and 10 Å, we could not obtain a reliable fit.

Water dipole orientation in the NPT and NVE simulations. We examined the orientation of water molecules within the SecY channel in terms of the water orientational order parameter defined as $P_d(z) = \langle \cos\theta \rangle(z)$, where θ is the angle between the water dipole and the membrane normal. The θ value varies between 0° and 180°, hence $\cos\theta$ varies between −1 and 1. A random distribution of the water dipoles corresponds to the <cos *θ*>= 0; non-zero values of <cos *θ*> indicate a preferred dipole orientation. For the *NPT* simulation Sim1, we read 1400 frames in each of the time range analyzed: 0 to 0.15 μs, 0.15 to 0.3 μs, and 0.3 to 0.45 μs. We computed cos *θ* by averaging the results obtained every 100 frames. We then calculated the final average and represented it as a function of the membrane normal (Fig. 5A). The error bars represent the standard errors of the means. For the 120 *NVE* simulations, we read 5000 frames and computed cos *θ* by averaging the results obtained every 250 frames. We then calculated the

final average and represented it as a function of the position along the membrane normal in the left-hand panels of Fig. S8. The error bars represent the standard errors of means.

Lipid incursions inside SecY in the NPT and NVE simulations. In order to calculate the time-averaged number of acyl chain carbon atoms located inside the square prism enclosing SecY during Sim1 (Figure S3A), we read 1400 frames in each of the time range analyzed: 0 to 0.15 μs, 0.15 to 0.3 μs, and 0.3 to 0.45 μs. We computed the number of the acyl chain carbon atom by averaging the results every 250 frames. We then calculated the final average and represented the results as a function of the distance from the SecY center. The error bars represent the standard errors of the mean. In order to calculate the number of acyl chain carbon atoms located inside the SecY hydrophobic region, we considered the volume defined by the hydrophobic residue positions (Figure S3B) and we followed the procedure previously described. We performed the same analysis for Sim2 (Figure S5A-v) and Sim3 (S5B-v). We represented the time-averaged number of acyl chain carbon atoms located inside the square prism enclosing SecY calculated from the 120 *NVE* simulations in the right-hand panels of Fig. S8. We read 5000 frames and obtained the number of the acyl chain carbon atom by averaging the results every 250 frames. We then computed the final averages and we presented them as a function of the position along the membrane normal. We grouped together the results obtained from *NVE* simulations run at times $t < 0.15$ μs (Fig. S8, upper panels) and those obtained at times $t > 0.15$ μs (Fig. S8, lower panels).

Supplementary Tables

Table S1. MD simulations in the *NPT* ensemble. The first and the second columns respectively report the three independent *NPT* simulations Sim1, Sim2 and Sim3, and their lengths.

***NPT* simulations**	**Length (μsec)**
Sim1	0.45
Sim2	0.13
Sim3	0.13

Table S2. MD simulations in the *NVE* ensemble. Summary of the 120 *NVE* simulations from Sim1 carried out to examine water dynamics. We selected 8 independent configurations every 2 ns from the following 5 time ranges of Sim1: 2 to 16 ns, 60 to 74 ns, 104 to 118 ns, 302 to 316 ns, and 402 to 416 ns. The specific simulated systems are listed in the first column, the number of *NVE* runs for each time window for each system in the second, time interval at which configurations were saved in the third, and the length of each simulation in the fourth.

***NVE* simulations (from Sim1)**	***NVE* simulations *per* time window**	**interval (fs)**	**length (ps)**
SecY (***SecY***)	8 x 5	5	50
Frozen SecY (***SecY-fix***)	8 x 5	5	50
Frozen SecY and charges off (***SecY-vdw***)	8 x 5	5	50

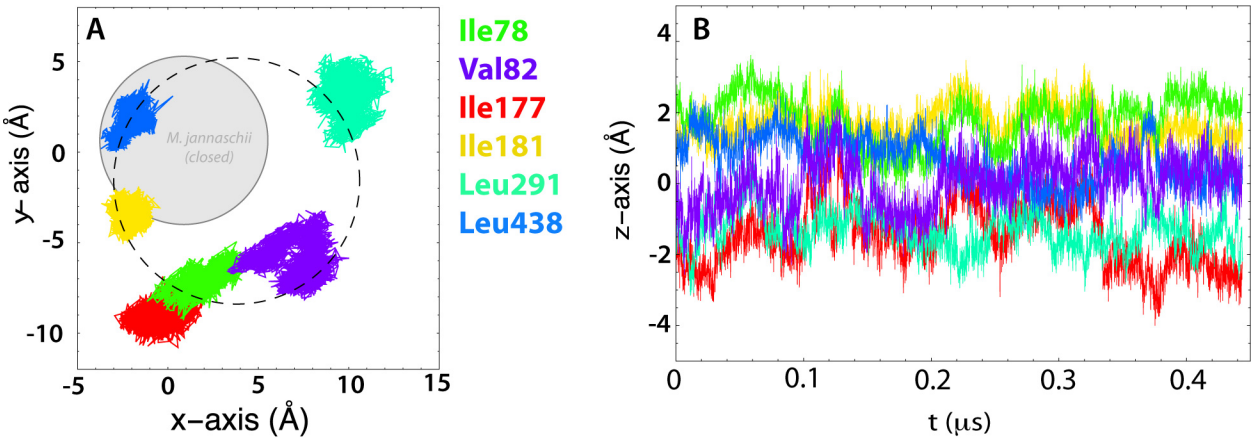

Figure S1. Dimensions of the 'primed' open hydrophobic ring (HR) of *P. furiosus* and the fluctuations of its six hydrophobic residues observed in Sim1. **A**. Time evolution of the centers-of-mass of the six HR sidechains projected onto the *xy* plane parallel to the lipid bilayer. The dashed circle through the time-evolution data represents the mean opening of the ring, calculated by fitting a circle through the points. The circle has a radius of 6.8±0.3 (s.d.) Å. Shown as a gray disk is the mean opening of the HR of the closed *M. jannaschii* SecYEβ (see Fig. S2). **B**. Time evolution of the centers-of-mass of the HR residues projected onto the *z*-axis.

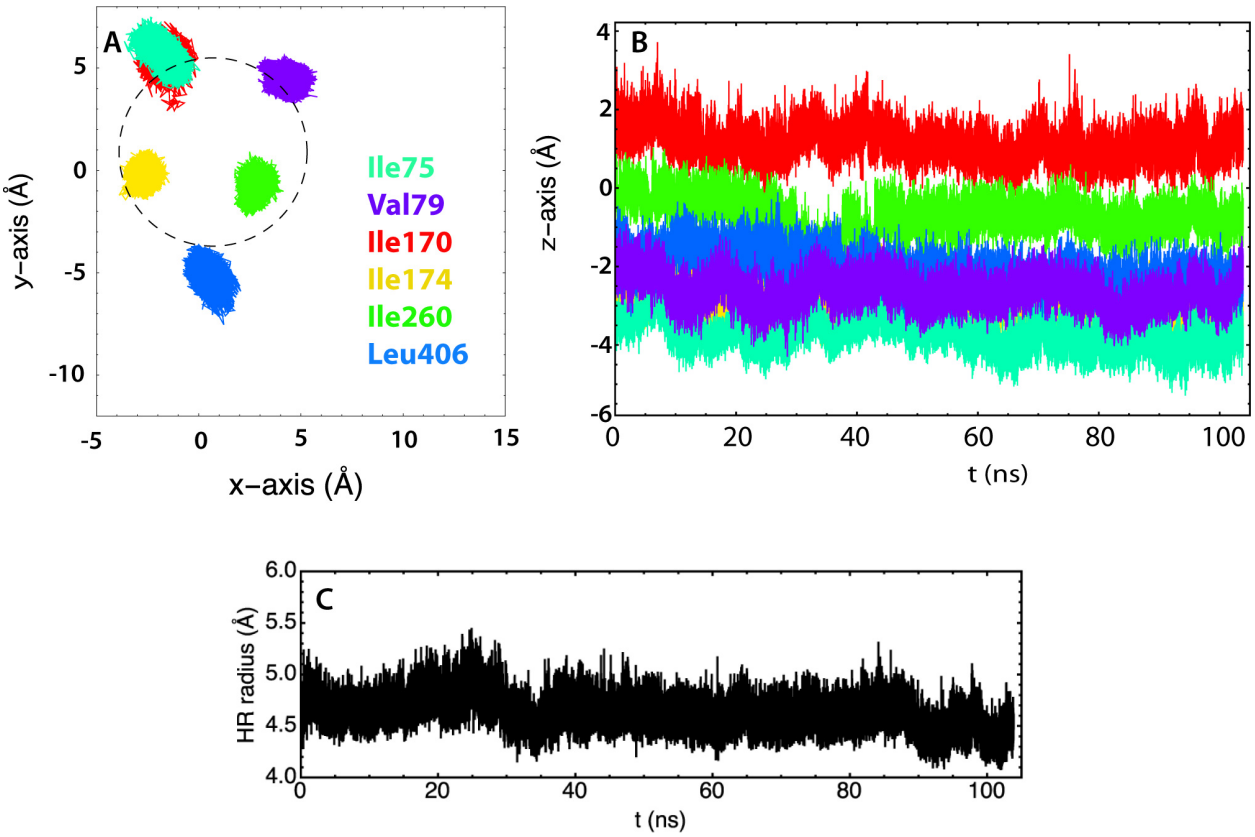

Figure S2. Dimensions of the closed hydrophobic ring (HR) of the SecYEβ translocon from *M. jannaschii* and the fluctuations of its six hydrophobic residues. **A**. Time evolution of the centers-of-mass of the hydrophobic residues projected onto the *xy* plane parallel to the lipid bilayer. The dashed circle through the time-evolution points represents the time-averaged opening of the HR obtained by fitting a circle through the points. The mean radius of the circle is 4.6±0.1 (s.d.) Å. **B**. Time evolution of the centers-of-mass of the HR residues projected onto the *z*-axis. **C**. Time evolution of the HR radius calculated over the entire length of the simulation.

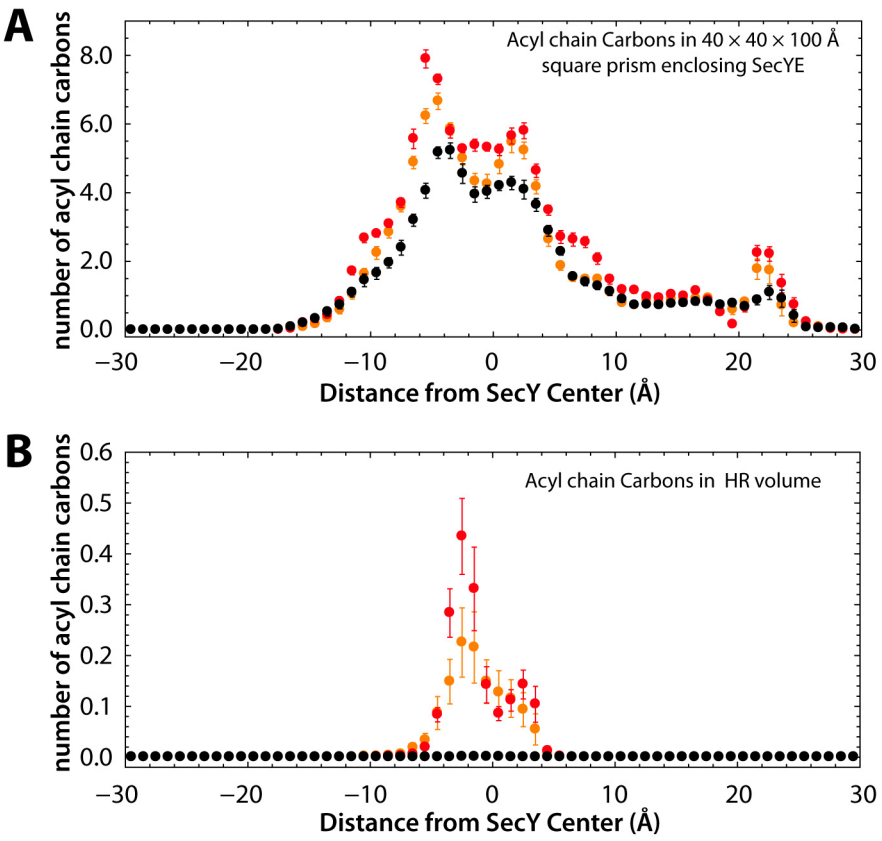

Figure S3. Average numbers of acyl chain carbon atoms within the aqueous interior of the SecYE translocon during Sim1 calculated by averaging over 1400 frames. The calculation was performed between 0 and 150 ns (*black* symbols), between 150 and 300 ns (*orange* symbols), and between 300 and 450 ns (*red* symbols). The error bars represent the standard errors of the mean. **A**. Number of acyl chain carbon atoms located inside the 40 Å × 40 Å × 100 Å square prism shown in Figure 2B. Overall, the acyl chain carbon atoms occupy less than the 2 % of the total volume of the prism. **B**. Average numbers of acyl chain carbons within HR region only, as defined by the hydrophobic residue positions (Fig. S1). Acyl chain carbons are absent or rarely found in the hydrophobic ring region. Note difference in vertical scale relative to panel A.

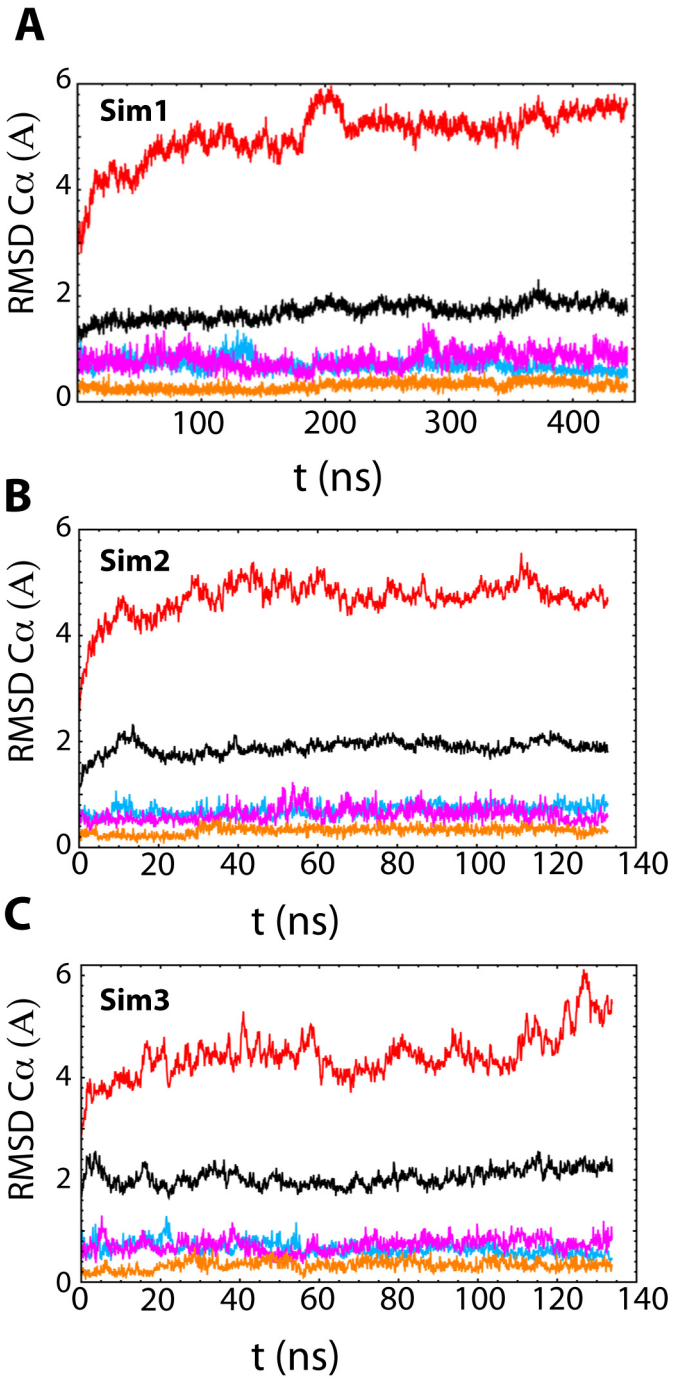

Figure S4. Time evolution of the root mean-squared deviations (RMSD) of SecYE from *P. furiosus* for the three *NPT* simulations presented in the paper. The panels show the time evolution of the RMSD of all the SecY C_α atoms (*red*), the SecY TM helices (*black*), TM2b (*magenta*), TM7 (*cyan*), and TM2a plug domain (o*range*) calculated from Sim1 **(A)**, Sim2 **(B),** and Sim3 **(C)**.

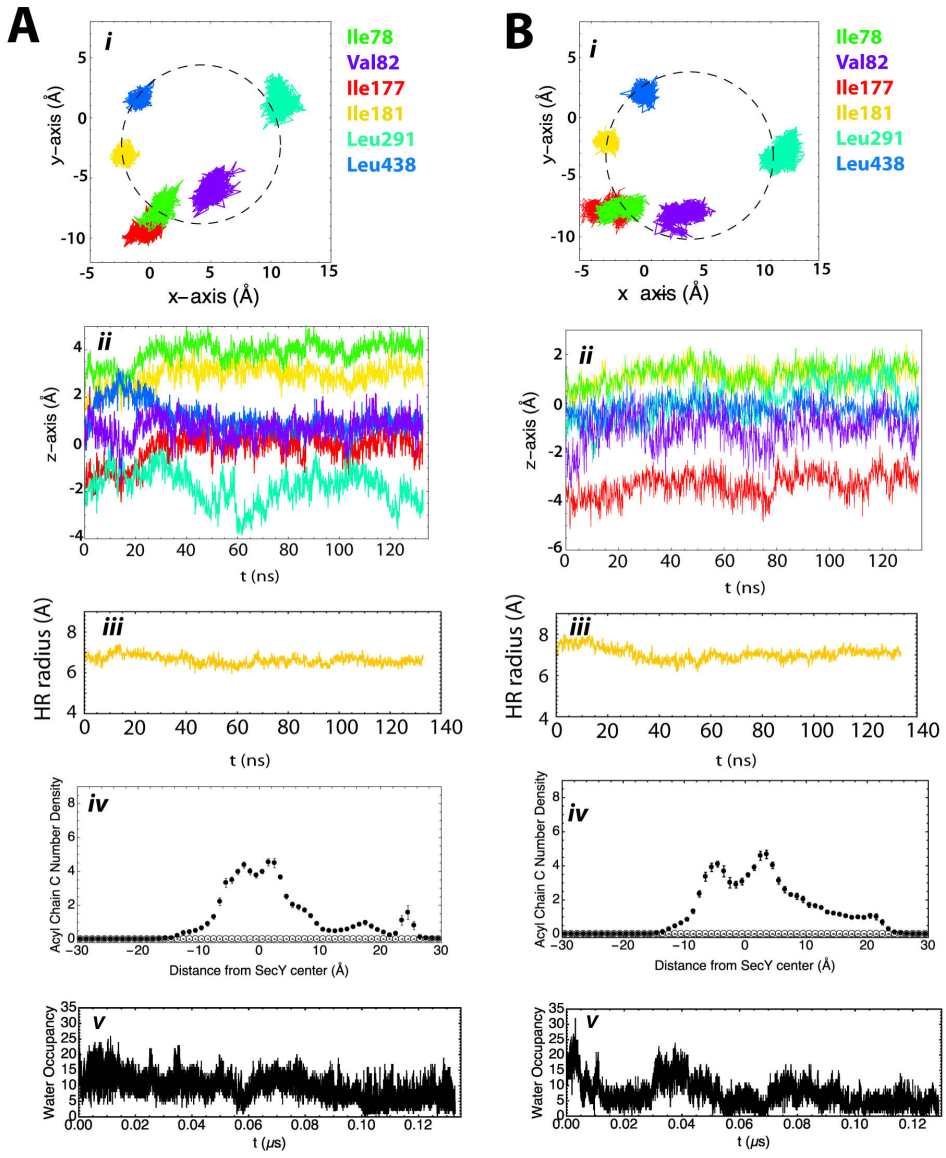

Figure S5. Summary of data obtained from Sim2 **(A)** and from Sim3 **(B)**. (***i***) The dashed circle through the time-evolution points represents the time-averaged opening of the HR obtained by fitting a circle through the centers of mass of the HR residues. The mean radius is 6.6±0.2 (s.d.) Å and 7.0±0.3 (s.d.) Å for Sim2 and Sim3, respectively. (***ii***) Time evolution of centers of mass of the hydrophobic residues projected onto the *z*-axis. (***iii***) Time evolution of the HR radius calculated over the entire length of the simulation. (***iv***) Time-averaged number of acyl chain carbon atoms located within the 40 Å × 40 Å × 100 Å square prism (*solid circle* symbols) and in the hydrophobic region as defined by hydrophobic ring residues (*empty circle* symbols). The error bars represent standard errors of the mean. (***v***) Time evolution of the water occupancy in the region enclosed by the six hydrophobic ring residues.

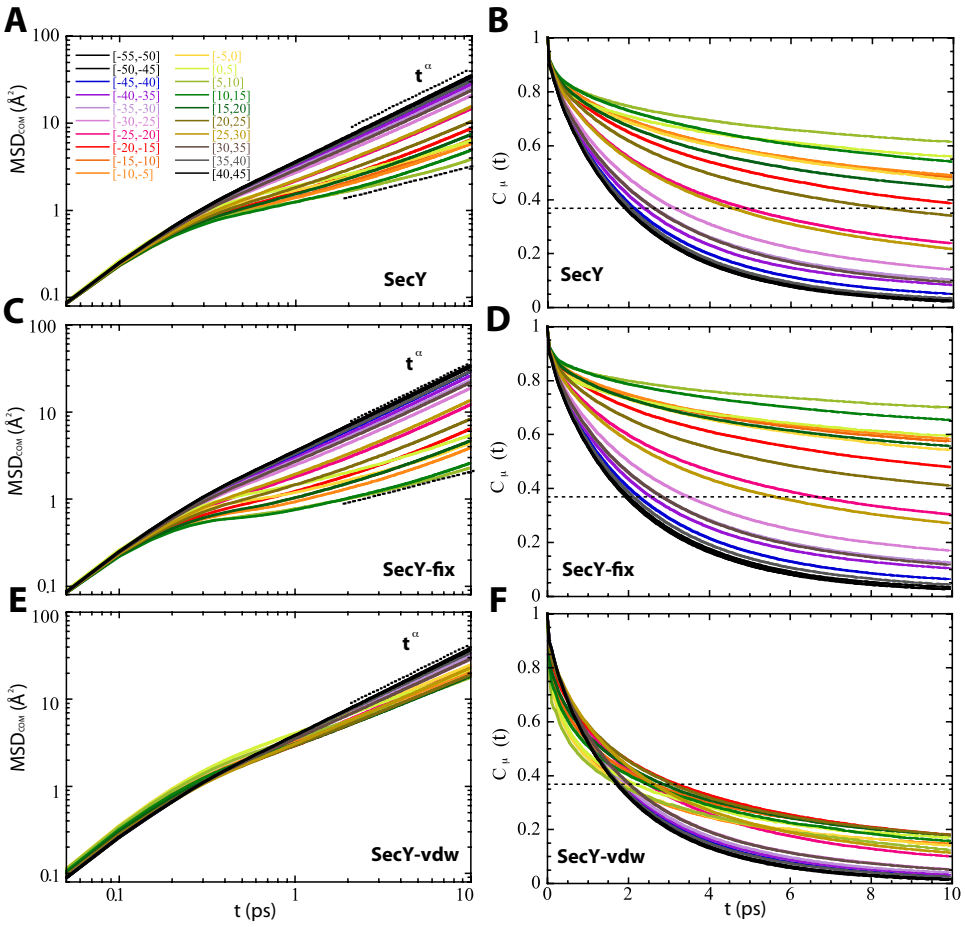

Figure S6. Time evolution of the mean squared displacements (MSD) and of the single-molecule dipole autocorrelation functions (SDAC). The results, averaged over the three types of *NVE* simulations carried out at times t < 0.15 μs, are shown under three conditions (see Methods): no restraints, *SecY*. Coördinates fixed, *SecY-fix*. Coördinates fixed and the SecY charges (including partial charges) turned off, *SecY-vdw*. Time evolution of the MSDs and SDACs are shown in the left-hand and right-hand panels, respectively. **A** and **B**, *SecY*. **C** and **D**, *SecY-fix*. **E** and **F**, *SecY-vdw*. The curves are colored according to the legends within the MSD plots describing the position along the membrane normal of the analyzed slab. The black line corresponds to water outside SecY, and the colored lines to water inside SecY. The time dependence of the MSD in the long-time regime was determined from the power function t^{α} (see Methods). The dashed lines in the SDAC plots correspond to the value 1/e.

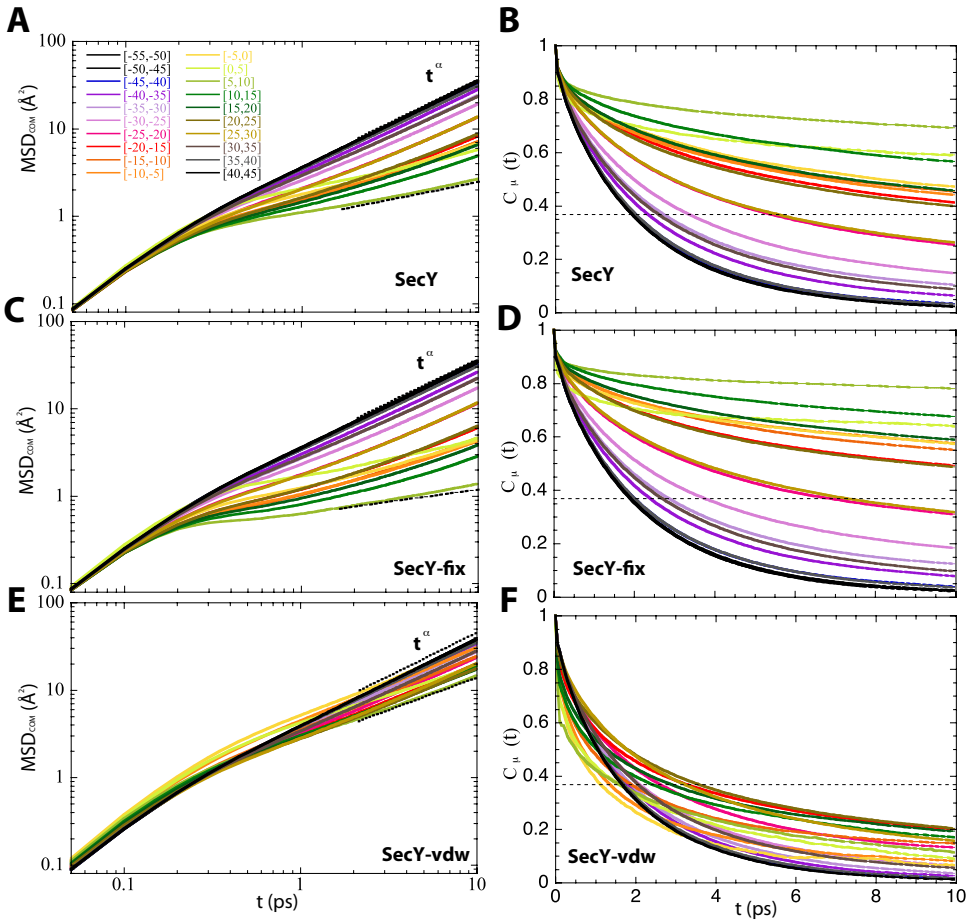

Figure S7. Time evolution of the mean squared displacements (MSD) and of the single molecule dipole autocorrelation functions (SDAC). The results, averaged over the two *NVE* simulations carried out at times t > 0.15 μs, are shown under three conditions (see Methods): no restraints, *SecY*. Coördinates fixed, *SecY-fix*. Coördinates fixed and the SecY charges (including partial charges) turned off, *SecY-vdw*. Time evolution of the MSDs and SDACs are shown in the left-hand and right-hand panels, respectively. **A** and **B**, *SecY*. **C** and **D**, *SecY-fix*. **E** and **F**, *SecY-vdw*. The curves are colored according to the legends within the MSD plots describing the position along the membrane normal of the analyzed slab. The black line corresponds to water outside SecY, and the colored lines to water inside SecY. The time dependence of the MSD in the long-time regime was determined from the power function t^α (see Methods). The dashed lines in the SDAC plots correspond to the value 1/e.

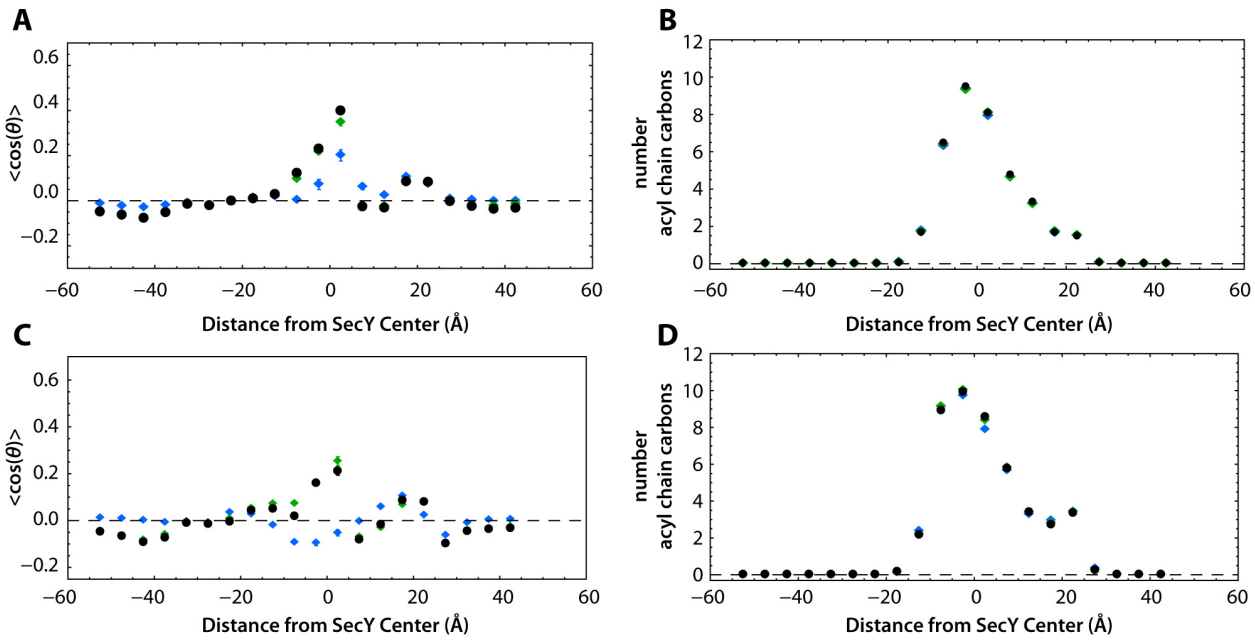

Figure S8. The effect of acyl chains on the alignment of water dipoles (left-hand panels) and number of acyl chain carbon atoms (right-hand panels) calculated from the *NVE* simulations. The results are shown for simulations under three conditions (see Methods): no restraints *(black symbols*), coördinates fixed *(green symbols*), and coördinates fixed and the SecY charges (including partial charges) turned off *(blue symbols*). The upper panels (**A** and **B**) show the results obtained from the *NVE* simulations carried out at time t < 0.15 μs, while the lower panels (**C** and **D**) show those obtained from the *NVE* carried out at time t > 0.15 μs.

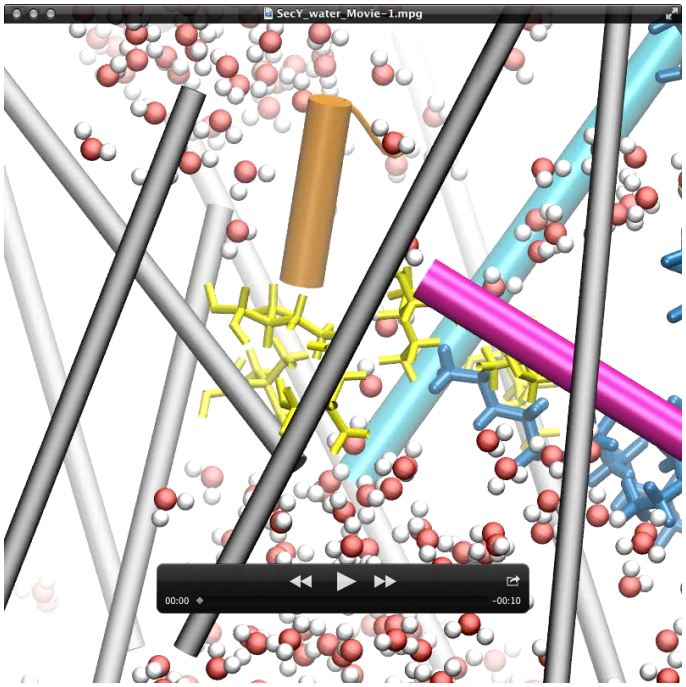

Movie 1. Passage of water molecules through the *Pyrococcus furiosus* SecYE translocon. The movie is derived from the water movement captured in Sim1. The movie shows 1.5 ns of the simulation starting at the 276.8 ns point of Sim1. Shown above is the first frame of the movie.

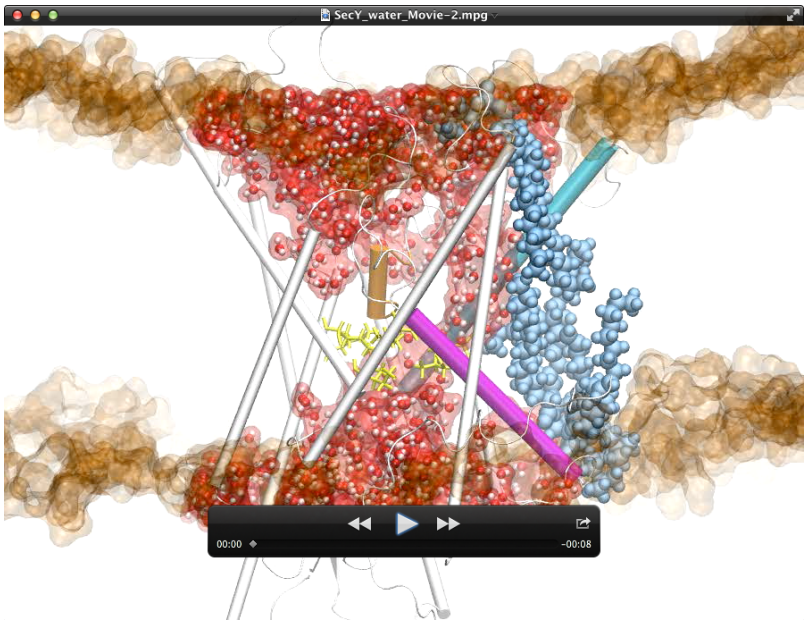

Movie 2. Images of the lipids at the front of the lateral gate of SecYE not interfering with water movement in the vicinity of the hydrophobic ring. The movie shows the structure of SecYE and

the lipids as SecYE is rotated about the *z*-axis. The movie is essentially a rotating view of Fig. 3B. Shown above is the first frame of the movie.

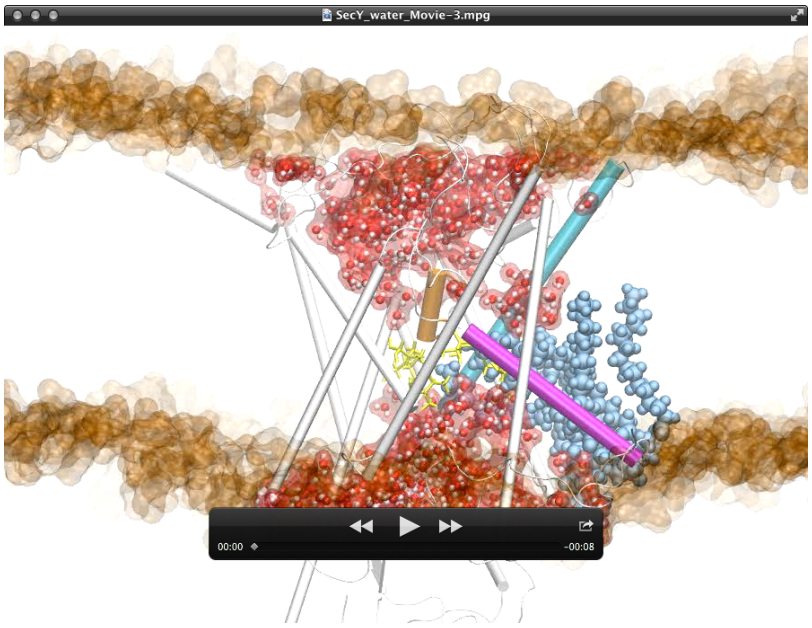

Movie 3. Images of the lipids at the front of the lateral gate of SecYE interfering with water movement in the vicinity of the hydrophobic ring. The movie shows the structure of SecYE and the lipids as SecYE is rotated about the *z*-axis. The movie is essentially a rotating view of Fig. 3C. Shown above is the first frame of the movie.

References

1. Egea PF & Stroud RM (2010) Lateral opening of a translocon upon entry of protein suggests the mechanism of insertion into membranes. *Proc Natl Acad Sci USA* 107:17182-17187.

2. Kelly LA & Sternberg MJE (2009) Protein structure prediction on the web: a case study using the phyre server. *Nature Protocols* 4:363.

3. Humphrey W, Dalke W, & Schulten K (1996) VMD: Visual molecular dynamics. *J Mol Graph* 14:33-38.

4. Van den Berg B*, et al.* (2004) X-ray structure of a protein-conducting channel. *Nature* 427:36-44.

5. Bizzarri AR, Rocchi C, & Cannistraro S (1996) Origin of the anomalous diffusion observed by MD simulation at the protein-water interface. *Chemical Physics Letters* 263:559-566.

6. Sengupta N, Jaud S, & Tobias DJ (2008) Hydration dynamics in a partially denatured ensemble of the globular protein human α-lactalbumin investigated with molecular dynamics simulations. *Biophys J* 95:5257-5267.